Rotating deep annulus convection. Part 2. Wave instabilities, vertical stratification, and associated theories

By JACK A. C. KAISER, *Hydrodynamics Laboratory, Department of the Geophysical Sciences, The University of Chicago, Chicago, Illinois 60637*

(Manuscript received January 28, 1969; revised version July 18, 1969)

ABSTRACT

The baroclinic instability theories which are relevant to the differentially heated, rotating annulus are reviewed and recalculated in a way which brings out the importance of the vertical stratification of the fluid. Experimental measurements of the wave-regime neutral surface are presented which qualitatively agree with most of the predictions of the theories; in particular, good agreement with the predicted effect of the vertical stratification is obtained. Some details concerning an observed transition from high amplitude waves to low amplitude waves are given. Also some experimental evidence on the existence of a one-wave mode and a mixed one-wave and two-wave mode is presented.

1. Introduction

In a previous paper, Kaiser (1969) (hereafter referred to as "I"), the thermal properties of the symmetrical regimes of flow observed in a rotating differentially heated annulus of fluid were discussed. A flow, either symmetrical about the axis of rotation, or of a wavelike nature is observed. The occurrence of these regimes is governed by the values of a gap thermal Rossby number, $\mathrm{Ro}_g \equiv gd\mathrm{Er}/2\Omega^2\Delta r^2$, and a Taylor number, $T_g \equiv 4\Omega^2\Delta r^4/\nu^2$, where g is the local gravitational acceleration; d, the fluid depth; Er, an unspecified horizontal fractional specific volume difference; Ω, the rotation rate; Δr, the gap; and ν, the viscosity of the fluid at the mid-point.

Several years ago it came to the attention of this author that Brindley's (1960) computations, when plotted in a T_g, Ro_g-plane (Fowlis, 1964), produced a diagram quite similar in many respects to the spectrum diagrams which had been obtained by Fultz (1964). At that time there was sufficient rudimentary experimental evidence (Fultz, 1964) to indicate that the vertical stratification parameter, $\mathrm{Sz}_g (= gd\mathrm{Ez}/2\Omega^2\Delta r^2$, Ez being the overall vertical fractional specific volume difference), is probably as important a parameter as Ro_g and T_g in determining the nature of the observed flow. The instability theories were recalculated so that the neutral surfaces for each wave number could be displayed in a T_g, Sz_g, Ro_g-space. The published material does not exhibit this dependence in usable form.

Then experimental spectral measurements were made to compare with the above-mentioned aspects of the theories. The results lend strong credence to the qualitatively comparable predictions of most of the theories. Also a transition from a high-amplitude to a low-amplitude wave regime was investigated along with the question of the existence of a one-wave mode.

The dimensions of the annulus are: $\Delta r = 2.442$ cm, $d = 13.00$ cm, and the radius of the inner cylinder is 2.456 cm. The upper surface is free, but a lid is positioned 2 cm above this free surface. The working fluid is distilled water with 0.1% by volume of a detergent.

2. A survey of the baroclinic instability theories

The various instability theories (Eady, 1949; Davies, 1956, 1959, Kuo, 1956; Brindley, 1960;

This material is part of a thesis submitted in partial fulfillment of the requirements for the Ph.D. degree in the Department of the Geophysical Sciences, The University of Chicago.

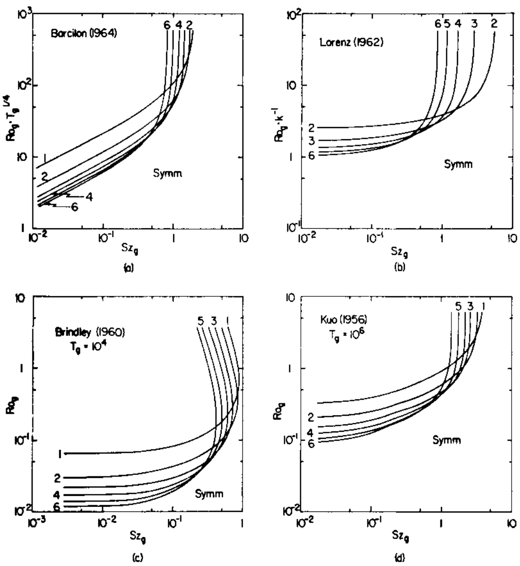

Fig. 1. Theoretical stability-variation curves for several wave numbers: (*a*) Barcilon (1964); (*b*) Lorenz (1962); (*c*) Brindley (1960), $T_g = 10^4$; and (*d*) Kuo (1956), $T_g = 10^6$.

Lorenz, 1962; Barcilon, 1964) examine the criterion for the stability of an infinitesimal wave-like perturbation on a very simplified basic state having linear or quadratic variations of density and zonal velocity both in the horizontal and vertical directions. In all cases approximate solutions are used. The theories also consider several different geometrical configurations as well as a variety of boundary conditions. Probably the most important distinction among the theories is the retention or neglect of viscous and thermal diffusive effects.

Both inviscid theories—Eady and Davies—give similar instability criteria: any particular wave becomes unstable below a critical value of the vertical stratification, the higher wave numbers becoming unstable at lower values of Sz_g, and there is, of course, no dependence on T_g.

When viscous and thermal diffusion effects are included, the simple results of the inviscid theories are drastically altered. For a fixed value of T_g, the Sz_g- constant criteria becomes strongly Ro_g-dependent for values of $Ro_g < 1$, and in most cases, at sufficiently low values of Ro_g, the neutral curves for each wave number are independent of Sz_g! Each neutral curve also has a strong dependence on T_g; thus forming a neutral surface. These three-dimensional spectra of Barcilon (1964), Lorenz (1962), Brindley (1960), and Kuo (1956) are illustrated in Fig. 1 for each wave number from 1 to 6 (Lorenz found wave number 1 stable for all values of the parameters). In all of these theories, if T_g is fixed, and Sz_g is sufficiently small, the neutral curve Ro_g-values continually decrease as the wave number is increased indicating that no particular wave number is most unstable; hence no one *maximum* wave number is predicted along any sizable portion of the envelope of the lower curves.

The inviscid theory instability curves are also contained in Fig. 1. Eady's results are just the upper vertical portions of Barcilon's curves, and Davies' neutral curves concide with the upper portions of those due to Brindley. Brindley's curves, for several values of T_g, are shown for wave number 4 in Fig. 2*a*—here Davies' curve for wave number 4 coincides with the $T_g = \infty$ curve. The set of Kuo's curves for wave number 1 are shown in Fig. 2*b*.

Under certain limiting conditions, the instability criteria of Davies, Brindley, Barcilon, and Eady all approach each other. This demonstrates a very important point: the inviscid theories appear to represent a regular limit point of the viscous theories!

All of the viscous theories do predict a spectrum diagram similar in some respects to those

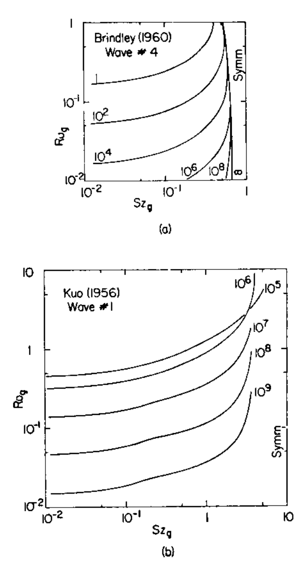

Fig. 2. Theoretical stability-variation curves for a fixed wave number: (*a*) Brindley (1960), $m = 4$; and (*b*) Kuo (1956), $m = 1$.

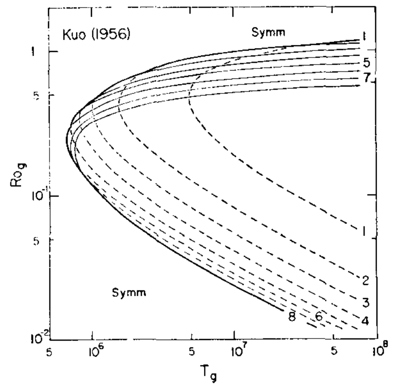

Fig. 3. The normal-stability spectrum constructed from the stability-variation curves of Kuo.

which have been determined experimentally (Fultz, 1959, 1964; Fowlis & Hide, 1965)—see also Fig. 6. Increasing $Ro_{g,w}$ from a small value corresponds to moving up and to the right along a line of positive slope in, say, Fig. 2*b*. First, the lower branch of a wave-number neutral curve is crossed, and as $Ro_{g,w}$ is increased to sufficiently large values, the upper branch is eventually crossed. From a diagram such as Fig. 2*b* one can see that, for a fixed wave number, below a certain value of T_g, this normal-stability line will not intersect the individual wave neutral curve, so each wave number will have a minimum value of T_g associated with it, and this marks the "knee" of the neutral curve in a T_g, Ro_g-plane.

Fig. 3, constructed from Kuo's theory, illustrates the spectrum diagram which results from the superposition of the wavenumber neutral curves. The upper and lower branches become respectively the upper and lower symmetry transition curves, and the wave regime neutral curve is the envelope of all the individual wavenumber transition curves (only wave numbers up to eight were considered for the diagram).

Fig. 4 is a composite of all the envelopes for the various theories constructed in the same manner as Fig. 3. The experimentally determined envelope is included for comparison. The "Davies (corr.)" curve in Fig. 4 is based on a viscous correction given in Davies (1956), whereas the other "Davies" curve does not have this correction. The lower symmetric portion of Davies' neutral curve is based on his 1959 paper.

Some question arises as to whether $Ro_{g,i}$ or $Ro_{g,w}$ is the better analogue to the Rossby number used in these theories. The theories assume basic states which do not have any thermal boundary layer structure on the vertical walls, whereas the measurements presented in (I) show pronounced boundary layer structure in the upper symmetric regime. For this reason, $Ro_{g,i}$ is probably the better analogue.

Why consider $Ro_{g,i}$ and Sz_g as independent parameters when any complete theory should predict both from the imposed conditions? First, no good complete theory presently exists—the problem is the lack of an accurate relation between $Ro_{g,i}$, Sz_g and the imposed conditions. Secondly, by considering the instability theories as applying to any reasonable flow in which $Ro_{g,i}$, Sz_g, and T_g are related differently than

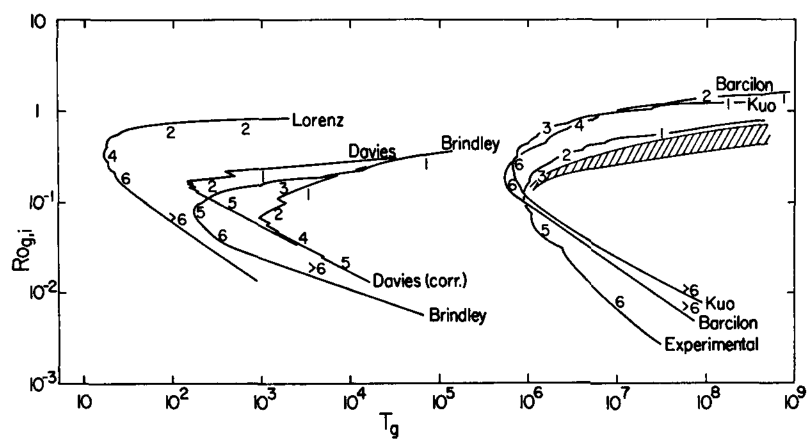

Fig. 4. The neutral curves from all the theories based on the experimentally determined relations between $Ro_{g,i}$ and Sz_g (see text). The numbers on the curves are the predicted wave numbers.

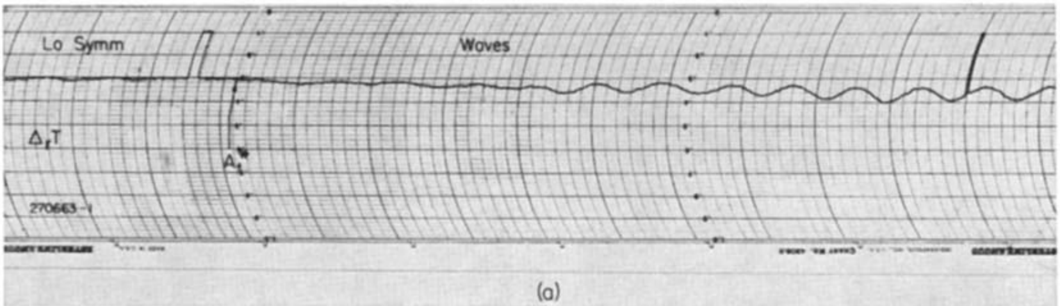

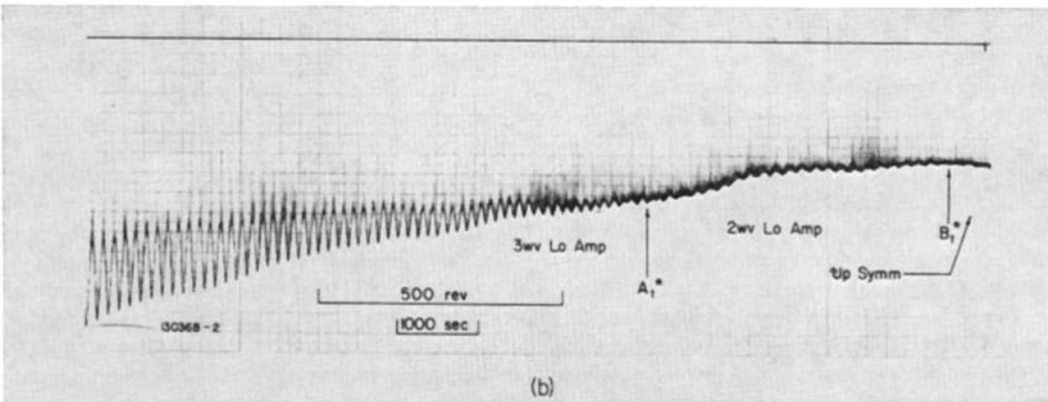

Fig. 5. Temperature traces from the fluid obtained as the wave-regime neutral curve is crossed. (*a*) A lower symmetric transition at 5.0 sec^{-1} ($T_g = 3.9 \times 10^7$) showing the onset of waves, and (*b*) an upper symmetric transition at 1.05 sec^{-1} ($T_g = 1.76 \times 10^6$) showing the gradual decay of waves.

in the annulus problem, the instability portion of the annulus theory has wider applicability. Thirdly, and most importantly, this author feels considerably more insight is shed on the phenomenon of baroclinic instability by separating the instability problem from the steady-state flow problem.

3. The experimental neutral curve

A careful mapping of the wave-regime neutral curve with a dense grouping of data points was obtained to bring out some of the fine scale features of this curve. The equipment and accuracy are the same as in (I). Great care was taken to obtain as nearly isothermal conditions as possible on each wall and the spatial deviations in temperature on each wall were generally under 5% of the imposed difference, except at values of $T_g > 10^8$ along the upper symmetry curve, where anomalies up to 11% were observed (the deviations on the working fluid side of the walls were significantly less than this). For most of the data, all the probes used in (I), which entered the fluid vertically, were removed because these probes tended to set off wave-like disturbances, particularly in the knee and lower symmetric regions. These disturbances were quite irregular compared to the normal baroclinic waves; but sufficiently deceptive that an erroneous neutral curve was obtained before the problem was realized and eliminated. Along the upper symmetric transition curve away from the knee region, the presence or absence of these probes produced little if any detectable change in the determination of the transition points between the wave and symmetric regimes.

The instability theories consider an infinitesimal perturbation superimposed on the basic state, and the experimental procedure used to obtain the transition points is one which essentially follows this same philosophy. The rotation of the apparatus remains constant through an experiment. Starting with a temperature difference below the critical value, it is slowly increased until the first definite indication of the desired transition occurs. The desired pattern may either develop and maintain itself or decay back to the original one. If the latter occurs, the temperature difference is again slowly increased until the transition is firmly established.

Temperature increase rates of less than 20% of the imposed temperature difference per hour were always used to insure quasi-steady-state conditions. The bulk of the transition data away from the lower symmetric transition curve was obtained with a 10% or less increase rate. This slow rate insured that the measured critical temperature difference for the transition was within 10% or less of the actual value, and reproducibility checks generally confirm this. Several transition points at the knee were obtained by decreasing the rotation rate in 1% steps every 5 min. The rotation decrease and temperature increase methods produce data reproducible and compatible to within 5%. The temperature increase procedure causes the experimental fluid to traverse an upward vertical path on Fig. 6, while the rotation decrease trajectory is upward and to the left along a line with a slope of -1 in a T_g, Ro_g-plane.

Fig. 5 illustrates these procedures and the nature of the instability when the neutral curve is very slowly crossed. Fig. 5*a* shows the temperature trace from the mid-point of the fluid at 5.0 sec^{-1} as a six-wave pattern gradually develops. The actual transition from the lower symmetric to the wave regime occurs at the point marked A_t^*—the temperature increase rate is 10% per hour. Fig. 5*b* illustrates the gradual decay of a three-wave pattern as the upper symmetric transition curve is crossed at a 7% per hour rate, the transition occurs somewhere in a small region centered on the point marked B_t^*. These traces illustrate the nature of the transitions to or from the symmetrical regimes, the sensitivity of the detectors, and the care used in obtaining all the transition data.

Following the procedure outlined above, about 70 high quality transition points were obtained along, and interior to, the wave-regime neutral curve. The normal-stability spectrum diagram resulting from this data is shown in Fig. 6. The solid circles represent transitions from the symmetrical to the wave regimes, the x's and triangles are for wave-to-wave transitions, and the open circles map out the transition from a high-amplitude to low-amplitude wave regime (see Section 5). The large numbers represent the wave numbers observed in the various portions of the wave regime. The gross features of this diagram are the same as the earlier ones of Fultz (1964).

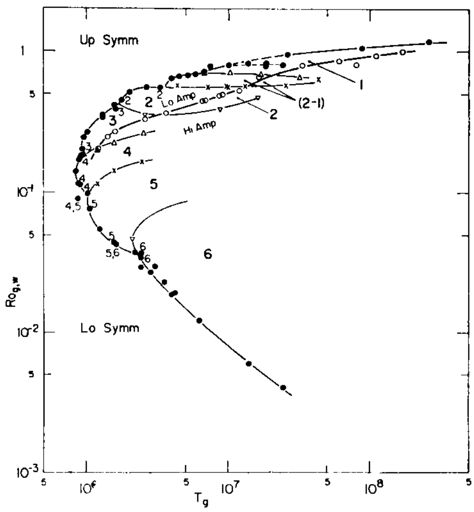

Fig. 6. Normal-stability neutral curve and a portion of the wave-regime spectrum based on $Ro_{g,w}$. The solid circles are the symmetry-wave transition points, the open circles are the high-amplitude–low-amplitude transitions, the inverted triangles are the six to five and three to two wave transition points, the x's are the five to four and two to (2-1) transition points and the triangles are the four to three and (2-1) to one transition points. The large numbers indicate the regions where the various wave modes occur and the small numbers are the wave numbers observed at those transition points.

One of the most interesting features of the wave regime neutral curve is the presence of cusps associated with a change of wave number. These generally went undetected in the earlier experimental work (Fultz, 1964; Fowlis, 1964, 1965) because the density of the data was not sufficient to establish definitely their existence. Since the transition data are reproducible to within 5 to 10% at all points around the neutral curve, and since these cusps represent about a 15% deviation from a smoothed transition curve, their existence is relatively certain.

Along the upper symmetry curve, near $T_g = 3 \times 10^7$, the upper symmetric transition data indicates an apparent zero-order discontinuity.

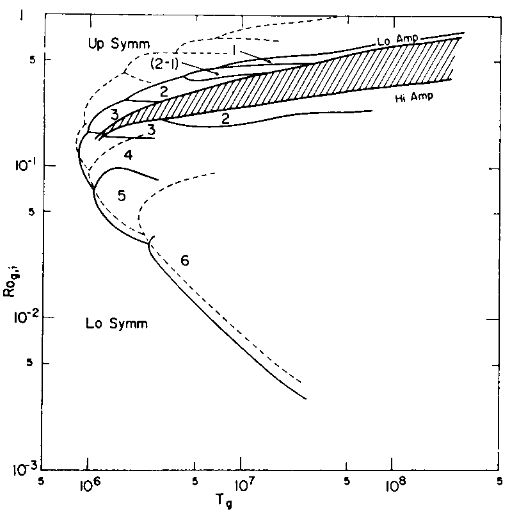

Fig. 7. The normal-stability neutral curve of Fig. 6 converted to $Ro_{g,i}$ using the relations found in (I). The shaded region is the high-low amplitude transition and the faint dashed spectrum is that of Fig. 6.

The wave regime neutral curve is broken to indicate this uncertainty, and the faint dashed curve merely suggests a possible alternative. There was no change in wave mode associated with the transition points on either side of this apparent discontinuity, so no cusp is indicated. What the nature of this discontinuity is, is unknown.

In all cases, the cusps are definitely associated with a wave-number change. In several cases, while occupying the transition points which are at the apex of the cusp, the fluid displayed either a top surface pattern or internal temperature trace which had some characteristics of both of the wave modes associated with the cusp. Lorenz (1962) stresses the importance of these cusps: "They would lend support to the hypothesis that the transition curve is composed of segments of transition curves for individual wave numbers."

The wave-number transition curves just inside the neutral curve appear to be extensions of the individual neutral curves for each wave number and, of course, emanate from the corresponding wave-number discontinuity on the neutral curve. They appear to correspond to the solid portion of the individual wave-number neutral curves of Fig. 3 in the sense of approximating a nonlinear instability theory by a linearized theory. A few transition points in the wave regime near the neutral curve were obtained by slowly *decreasing* the imposed temperature difference. This causes a transition to a higher wave number (in the temperature increase case, the wave number decreases). The transition curves obtained (not shown in Fig. 6) also emanate from the same cusps as those of the increasing case, but they now have a strong resemblance to the dashed curves of Fig. 3—a downslope away from the cusp. Whether the upper portion of the wave regime neutral curve is crossed from above or below does not seem to produce much difference in the critical value. The increasing transitions occur at values of $Ro_{g,w}$ about 10% greater than for the decreasing case (Fultz, 1964). In the wave regime, away from the neutral curve, however, the corresponding differences can amount to several hundred percent.

As was pointed out before, $Ro_{g,i}$ is probably a better analogue than is $Ro_{g,w}$ to the thermal Rossby number used in the theories because of the existence of the side-wall boundary layers. Using the results given in I and additional information concerning the relation of $Ro_{g,i}$ to $Ro_{g,w}$ along the periphery of the wave regime, a T_g, $Ro_{g,i}$-spectrum (Fig. 7) was constructed from Fig. 6—the dashed curve of Fig. 7 is the $Ro_{g,w}$-spectrum. The most interesting feature is the transformation of the high-low amplitude transition curve into a zone (shaded in Fig. 7). This unusual transition will be described in Section 5.

A set of temperature profiles obtained along the upper symmetric transition curve is shown Fig. 8. The dashed curves represent the scaled temperature field and the solid curves the scaled specific volume field (0 is the outer well temperature and 10 the inner wall temperature). As can be seen, the temperature field in the fluid has much more "structure" than the relatively simple basic states treated by the instability theories. Because of this, any detailed quantitative comparisons between theory and experiment are probably not too meaningful. The various theories predict values of Sz_g from 0.90 to 5.40 for the upper symmetry curve, and experimentally ($T_g > 10^7$) the vertically averaged value of Sz_g is 1.3 while the local maximum value is 3.6 for the upper symmetry transition. It is interesting to note that, for $T_g \geqslant 10^6$, the internal isotherm slope in the fluid varies by only 6% along the upper symmetric transition curve.

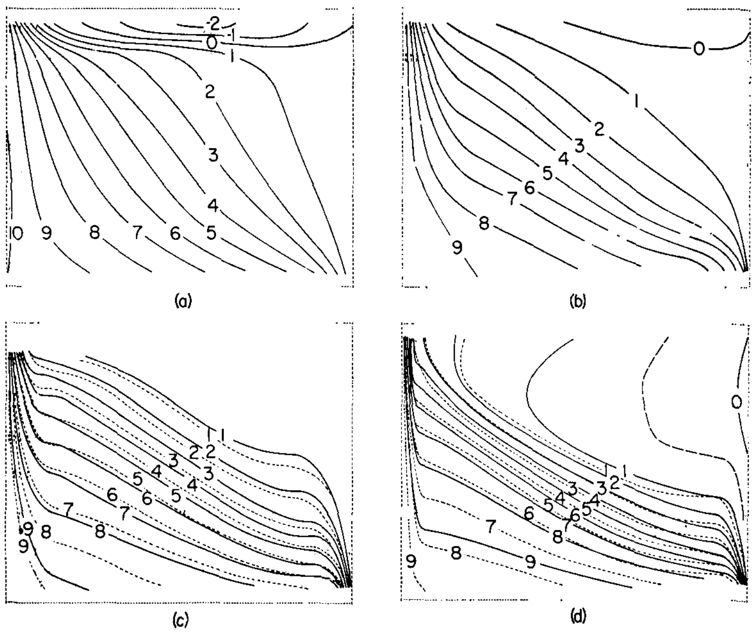

Fig. 8. Specific volume profiles obtained adjacent to the neutral curve: (*a*) at the knee, $\Omega = 0.69$ sec^{-1}, $T_g = 7.5 \times 10^5$, $Ro_{g,w} = 0.148$, $\Delta r_w T = 0.30$°C; (*b*) $\Omega = 1.00$ sec^{-1}, $T_g = 1.5 \times 10^6$, $Ro_{g,w} = 0.416$, $\Delta r_w T = 1.80$°C; (*c*) $\Omega = 2.00$ sec^{-1}, $T_g = 7.6 \times 10^6$, $Ro_{g,w} = 0.804$, $\Delta r_w T = 13.74$°C; and (*d*) $\Omega = 5.00$ sec^{-1}, $T_g = 2.6 \times 10^8$, $Ro_{g,w} = 1.10$, $\Delta r_w T = 68.14$°C. In cases (*c*) and (*d*) the dashed lines are the corresponding temperature fields. $\Delta r_w T$ is the imposed wall-to-wall temperature difference.

4. An Sz_g, Ro_g-cross section of spectrum space

At one rotation rate—1.0 s^{-1}, $T_g = 1.55 \times 10^6$—the vertical stability of the fluid was increased over its normal value by imposing equal positive temperature gradients on each cylinder wall. This was accomplished by electrical heaters placed in each bath near the cylinders and extending most of the vertical extent of the cylinders. As the bath liquid is forced to flow up past each heater it is gradually warmed producing the desired vertical gradients on the cylinder walls. The wattage dissipated by each heater was adjusted until the temperature difference across the cylinders was nearly equal near the *top, bottom,* and at *mid-depth.* Flow rates of 63 cc sec^{-1} were used for each bath.

This scheme actually worked very well as the profile of Fig. 9 demonstrates. In the normal-stability case (isothermal cylinder walls), the vertical temperature difference on the working fluid side of each cylinder was about 10% of the bath difference. In the high-stability case of Fig. 9, the vertical temperature difference on each wall was increased to 55% of the bath temperature difference! For this profile, the bath temperature difference was about 0.5°C, and 200 w of heat was dissipated by each heater.

The experimental technique used to obtain the stability-variation spectrum was essentially the same as that used for the normal stability case—a slow controlled differential temperature

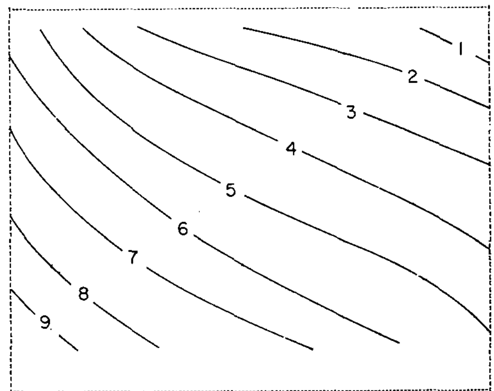

Fig. 9. High-stability specific volume profile. $\Omega = 1.00$ sec^{-1}, $T_g = 1.5 \times 10^6$, $Ro_{g,w} = 0.047$, and $Sz_g = 0.0313$.

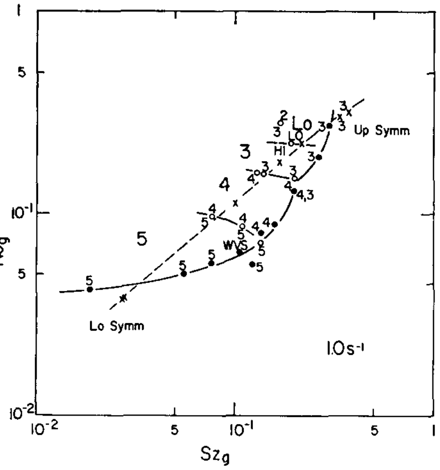

Fig. 10. Stability-variation spectrum at 1.00 sec^{-1}. The solid circles are the symmetry-wave transition points, the open circles are the wave regime transition points, and the x's are the normal-stability transition points obtained with the bath configuration used in (I). The dashed line is the normal stability relation for this case and the numbers are the observed wave numbers.

increase at rates of 20% per hour or less. The power to the heaters in each bath was set well before the occurrence of the desired transition.

The results of these altered stability runs are summarized in the spectrum diagram of Fig. 10. Ro_g is the thermal Rossby number used by Fultz (1964) in his older work and lies intermediate between $Ro_{g,w}$ and $Ro_{g,i}$, although the high-stability profile of Fig. 9 indicates that it would be very close to $Ro_{g,i}$ for most of this data. Sz_g is a vertical difference measured at the mid-gap. The dashed curve is the normal-stability relation at 1.0 s^{-1}, and the x's are the transition points obtained with the bath configuration used for all the normal-stability data (e.g., for Fig. 6). The solid circles represent the transition points between the symmetric and wave regimes, the open circles are some wave transition points, and the numbers represent the wave numbers observed.

This stability-variation spectrum agrees qualitatively, especially in the knee region, with the similar type of theoretical diagram obtained from Kuo's, Lorenz', and Brindley's theories (see Fig. 1) but disagrees with Barcilon's lower symmetry behavior. The lower symmetric transition curve becomes almost independent of Sz_g at sufficiently small values of Sz_g, and the upper symmetric transition curve appears to be rapidly approaching a dependence on Sz_g only, as the theory predicts. The importance of Fig. 10 lies in the qualitative agreement with the theoretical Ro_g, Sz_g-diagrams.

5. The high-amplitude, low-amplitude wave transition

The "high-low" transition displays characteristics quite different from all the other regime and wave-number transitions, and it most certainly appears to be of fundamental and "operational" importance.

Let us consider what happens as the imposed temperature difference is slowly increased through a range in which the high–low transition occurs. Starting in the high-amplitude wave regime, very obvious wave motions are present. The top surface tracer (fine aluminum powder) shows strong radial flow from the inner to outer cylinder in the jet band associated with the wave motion. The temperature records from all portions of the fluid also show large amplitude wave motions—the thermal contrast across these waves at ($\bar{r}$, $d/2$) is a sizeable fraction of the imposed horizontal temperature difference. As the transition is crossed, the high-amplitude wave motions decay within the time required for several waves to pass a fixed point, and the top-surface aluminum powder band suddenly gives all the appearances of a symmetric flow; however the temperature records from the interior of the fluid still show wave motions, but of a much reduced amplitude.

A set of temperature records from the midpoint of the fluid, obtained as the high-low transition is crossed, is shown in Fig. 11. The upper left trace is in the knee region and the transition occurs at the point marked B_t. The "thermal amplitude" of the waves decreases by about a factor of 3 and the mid-point warms up slightly. As we progress to higher rotation rates, the before–after amplitude ratio increases until at 4.0 s^{-1} ($T_g = 7.3 \times 10^7$, lower left trace) this ratio is about 10. At values of $T_g \geqslant 2 \times 10^7$, the midpoint temperature of the coldest portion of the wave in the low-amplitude regime actually becomes warmer than the mid-point temperature of the warmest portion of the wave observed in the high-amplitude wave regime just before the transition. The lower right-hand temperature record is for a low-amplitude to high-amplitude transition which was obtained by decreasing the

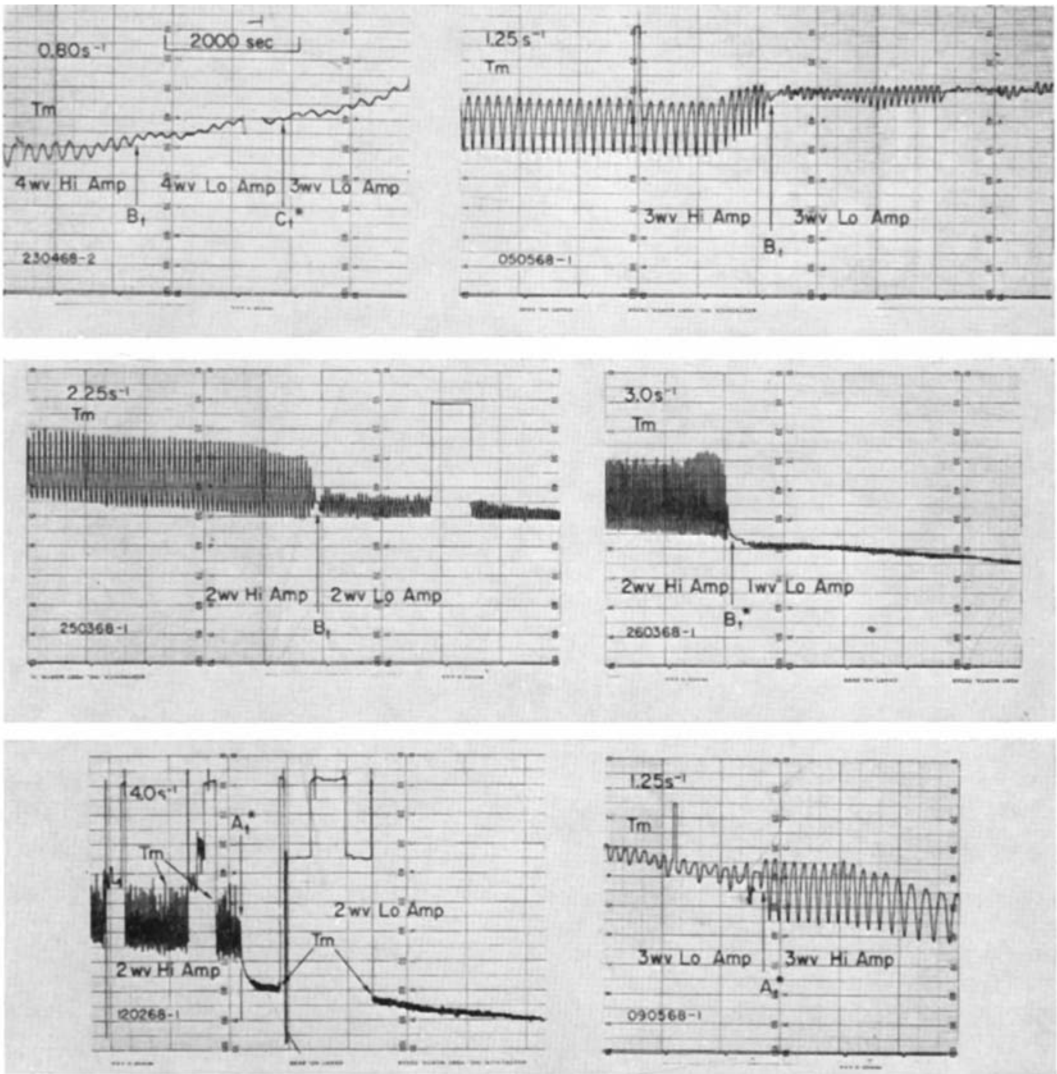

Fig. 11. Temperature records from the mid-point of the fluid obtained while traversing the high–low amplitude transition. All traverses are from high to low amplitude except that in the lower right, which is from low to high amplitude.

imposed temperature difference. The rotation rate is the same as that for the upper right-hand chart. This illustrates that in going from low- to high-amplitude waves, the high–low amplitude sequence of events is reversed, except at about 10% lower values of $\mathrm{Ro}_{g,w}$. There is continuity of wave number across the high–low transition except in the small regions where the wave number transition curves intersect the high–low transition curve (see Fig. 6).

The suddenness of this transition is matched only by transitions from one wave number to another, and this suggests that the high–low transition is a highly nonlinear phenomenon as probably the wave-number transitions are. The spectral changes to which the linearized theory appears to apply are those in which either a slow increase or decrease of amplitude is observed as the temperature difference is slowly changed (e.g., Fig. 5). The high–low transition is certainly not of this nature.

Two sets of specific volume profiles were ob-

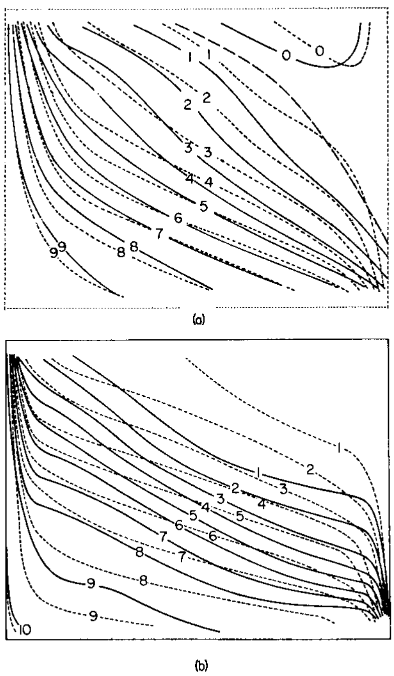

Fig. 12. Specific volume profiles on either side of the high-low-amplitude transition curve. The dashed lines are for the high-amplitude regime and the solid lines for either the low-amplitude (*a*) or upper symmetry regime (*b*): (*a*) 1.25 $\sec^{-1}$, $T_g = 2.5 \times 10^6$, $\mathrm{Ro}_{g,w} = 0.278$ and 0.337; (*b*) 3.00 $\sec^{-1}$, $T_g = 2.0 \times 10^7$, $\mathrm{Ro}_{g,w} = 0.536$ and 1.03.

tained on either side of the high–low transition curve and these are shown in Fig. 12. The dashed lines are for the high-amplitude regime and the solid lines for the low-amplitude regime (or upper symmetric regime in the case of Fig. 12 b). These profiles very clearly show the readjustment of the internal temperature field as the transition is crossed. In the low-amplitude regime, the longitudinally-averaged internal temperature fields are essentially the same as in the upper symmetric regime. This implies that the radial advection of heat by the wave component must be very small in the low–amplitude case. In the high-amplitude case there are strong radial heat transports which reduce the interior isotherm slope compared to the low-amplitude case.

The drastic changes observed at the free-surface as the high-low transition is crossed might suggest some change in the modal structure of the waves, such as an increase in the "wave number" in the vertical. The amplitude of the thermal oscillation due to the wave propagation past a meridian plane, as a function of r and z, is shown in Figs. 13*a* and *b* for the low- and high–amplitude regimes respectively. Both regimes show essentially the same structure—a band of maximum amplitude extending from the lower-outer to the upper-inner cylinder. Thus, the evidence strongly suggests there are no additional internal nodal surfaces present within the fluid in the low-amplitude case and, in fact, no modal structure change at all occurs in crossing the transition.

The sudden reorientation of the interior temperature field as the high-low transition is crossed is responsible for the "opening up" of the high-low *curve* of Fig. 6 into the shaded zone of Fig. 7. As the high–low transition is crossed from below, $\mathrm{Ro}_{g,t}$ suddenly jumps from the bottom to the top of this "forbidden region". The magnitude of this jump increases with increasing T_g, and at $T_g = 10^8$, it is 85%. Below $T_g = 10^6$, this transition is not detectable, probably because the changes associated with it are quite small.

Several investigators (Fowlis, 1964; Fowlis & Hide, 1965; Lambert & Snyder, 1966) have probably reported the high–low transition as the transition separating the upper symmetric and the wave regimes. Fowlis & Hide appar-

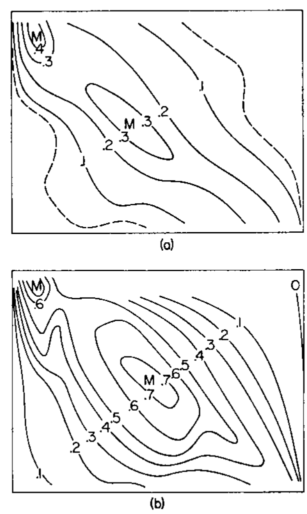

Fig. 13. Thermal amplitude fields of the waves corresponding to the profiles of Fig. 13*a*. (*a*) The low-amplitude wave regime and (*b*) the high-amplitude wave regime. The isopleths are in °C. Scaled with respect to the wall temperature difference, the amplitude ratio (high- to low-amplitude) is 3.

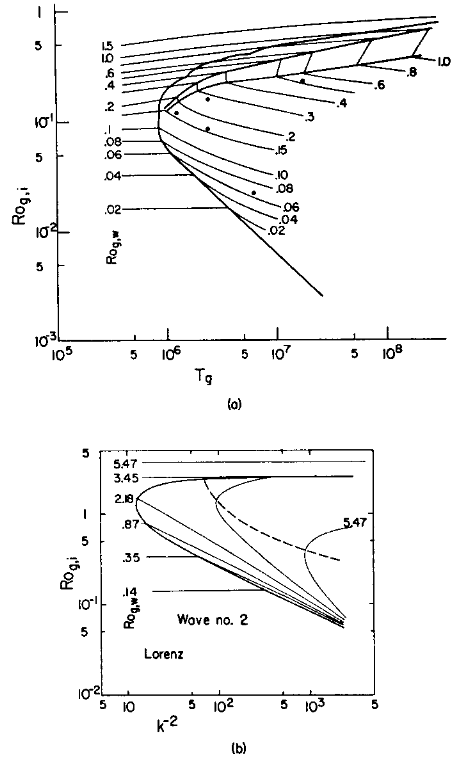

Fig. 14. (*a*) Measured $Ro_{g,w}$-field in the symmetric regime and portions of the wave regimes. (*b*) Theory due to Lorenz (1962) relating the internal to external Rossby number for wave number 2.

ently determined the identity of the various regimes by visual observations of the free surface (they had no temperature detectors in the working fluid), and the properties of the low-amplitude regime would indicate that, visually, the high–low transition would appear to be the upper symmetric transition, except possibly in the knee region where some marginal vestiges of waves occasionally can be detected in the low-amplitude regime. Lambert & Snyder (1966) explicitly describe the onset of waves from the upper symmetric regime, and their description precisely fits that given here for the high–low transition. All of Fultz's (1959, 1964) older work was carried out with thermocouples in the fluid, and what was reported by him as the upper symmetric transition is the transition from the low amplitude regime to the upper symmetric regime.

One theory (Lorenz, 1962) obtains sufficient detail in the Rossby regime concerning the thermal structure of the fluid so that something which may be analogous to the high–low transition appears. A comparison of the $Ro_{g,w}$-field in a T_g, $Ro_{g,i}$-plane, as measured experimentally and predicted by Lorenz, is given in Figs. 14 *a* and *b*. In both cases, the $Ro_{g,w}$-field is multivalued—in the experimental case the multivaluedness is associated directly with the high–low transition. Lorenz argues: as $Ro_{g,w}$ is increased from small values, $Ro_{g,i}$ also increases. As the dashed curve (Fig. 14*b*) is crossed, suddenly a smaller value of $Ro_{g,w}$ is sufficient to maintain the existing value of $Ro_{g,i}$, and a stability analysis for the wave regime above the dashed curve indicates that the wave perturbations are unstable. This argument would suggest, as the fluid reaches the dashed curve of Fig. 14, without a further increase in $Ro_{g,w}$, $Ro_{g,i}$ will spontaneously "jump" to the upper portion of the same $Ro_{g,w}$-isopleth which, in Lorenz' theory, lies on the neutral curve. This feature of Lorenz' theory may be due to the retention of some portion of the advection terms.

6. The (2-1)-wave and 1-wave modes

In the low-amplitude wave regime, at values of $T_g > 3 \times 10^6$, a "(2-1)-wave" and one-wave mode was encountered in the regions indicated on the spectrum diagram of Fig. 6. The one-wave mode has been previously reported (Fultz, 1959), but not documented. The (2-1)-wave mode appears to represent a mixture of a one- and two-wave mode.

Since these modes occur in the low-amplitude wave regime where visual detection of the modes is impossible, one has only temperature records to rely on for wave number identification, and then one must use the fact which Hide (1958) reported: the wave propagation rate, scaled with respect to $Ro_{g,w}$ is independent of the wave number. If we further assume that only integral wave numbers can exist in a quasi-steady-state, and this assumption appears well founded both theoretically and experimentally, then we can determine wave numbers from a temperature trace provided that, for one known wave number, the passage period is known.

Fig. 15 is a temperature record obtained near the midpoint of the fluid at $T_g = 10^7$ (2.25 sec^{-1}) as the fluid traverses the two-wave, (2-1)-wave, and one-wave regions. A_t marks the transition from the two-wave to the (2-1)-wave mode and

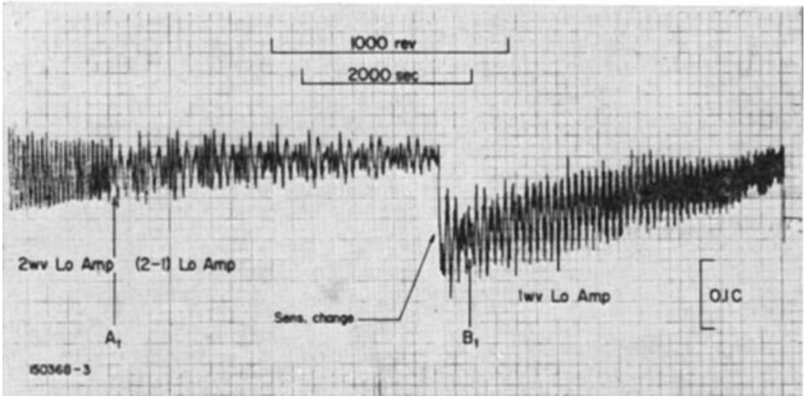

Fig. 15. An internal temperature record obtained as the two-wave, (2-1)-wave and one-wave regions are traversed at $\Omega = 2.25$ sec^{-1} ($T_g = 1.0 \times 10^7$).

B_t and transition from the (2-1)-wave to the one-wave mode. The two-wave pattern (even though in the low-amplitude region) was positively identified through continuity of the wave passage periods across the high–low transition. The wave passage periods of the segments of the apparent two-wave pattern just to the right of A_t are within 2% of the passage periods of the established two-wave mode to the left of A_t. The passage periods of the apparent one-wave portion of the (2-1) temperature record is very close to twice that of the two-wave portion of the (2-1)-wave mode. Also, the passage period of the one-wave portion of the (2-1)-wave record is within 5% of that of the apparent pure one-wave mode whose trace is to the right of B_t. The (2-1)-wave mode region could be considered as a zone of gradual transition between a regular two-wave pattern and a one-wave pattern.

7. Summary

For a proper understanding of the phenomenon of the baroclinic instability of a viscous fluid, it is vital that the vertical stratification be regarded as a parameter equal in importance to $Ro_{g,t}$ and T_g. In fact, the wave regime is bounded by a neutral surface in T_g, Sz_g, Ro_g-spectrum space.

At this stage only qualitative comparisons between theory and experiment appear meaningful. The cusped behavior and the Sz_g, Ro_g-cross section do indeed provide good agreement. All of the theories predict slopes of the lower symmetric transition curve of either $-\frac{1}{2}$ or $-\frac{1}{4}$ in the T_g, Ro_g-plane. The experimentally determined slope is close to -1. Also, the theory does not predict a single maximum wave number along a large segment of the lower symmetric transition curve whereas the experiments definitely show one to exist. The instability theories appear to have their greatest failure along the lower symmetric transition curve.

The instability theories considered here are a first attempt to explain certain features of the large-scale eddy motions of the atmosphere. Since they are also capable of explaining the stability properties of a physicaliy similar laboratory system—in which the response is much more precise than in the atmosphere—every effort is needed to accurately assess these theories for the laboratory experiments. When a theory evolves, which describes in detail *all* the aspects of the annulus experiments, then one can have a high degree of confidence that it will be equally useful in predicting the various states of the atmosphere when properly applied.

Acknowledgements

The author expresses his gratitude to Professor Dave Fultz for valuable guidance, Mrs Joyce Weil for programming, Mr Anthony Kordecki for assistance with the equipment, and Mr George Gray and Miss Mona Connor for preparation of the figures. Financial support from the Atmospheric Sciences Section of the National Science Foundation (grant GA-1023) and the Institutes for Environmental Research of the Environmental Sciences Services Administration (grant ESSA E22-107-67 G and grant ESSA E22-24-69(G)) is most gratefully acknowledged.

REFERENCES

Barcilon, V. 1964. Role of Ekman layers in the stability of the symmetrical regime obtained in a rotating annulus. *J. Atmos. Sci. 21*, 291–299.

Brindley, J. 1960. Stability of the flow in a rotating viscous incompressible fluid subject to differential heating. *Phil. Trans. Roy. Soc. London* (A) *253*, 1–25.

Charney, J. 1947. The dynamics of long waves in a baroclinic westerly current. *J. Meteor. 4*, 135–162.

Davies, T. V. 1956. The forced flow due to heating of a rotating liquid. *Phil. Trans. Roy. Soc. London* (A) *249*, 27–64.

Davies, T. V. 1959. On the forced motion due to heating of a deep rotating liquid in an annulus. *J. Fluid Mech. 5*, 593–621.

Eady, E. T. 1949. Long waves and cyclone waves. *Tellus 1*, 33–52.

Fowlis, W. 1964. An experimental study of the transitions between the flow regimes of thermal convection in a rotating annulus of liquid. Ph.D. dissertation, The Massachusetts Institute of Technology, 188 pp.

Fowlis, W. & Hide, R. 1965. Thermal convection in a rotating annulus of liquid: effect of viscosity on the transition between axisymmetric and nonaxisymmetric flow regimes. *J. Atmos. Sci. 22*, 541–558.

Fultz, D., Long, R., Owens, G., Bohan, W., Kaylor, R. & Weil, J. 1959. Studies of thermal convection in a rotating cylinder with some implications for large-scale atmospheric motions. *Meteor. Monogr. 4*, no. 21, 104 pp.

Fultz, D., Kaiser, J., Fain, M., Kaylor, R. & Weil, J. 1964. Experimental investigations of the spectrum of thermal convective motions in a rotating annulus. In Final Report, Research on Hydrodynamic Analogues of Large-Scale Meteorological Phenomena, AFCRL-64-382, Contract AF 19(604) -8361, April, U.S. Air Force Cambridge Research Laboratories, Office of Aerospace Research, U.S. Air Force, Bedford, Mass.

Hide, R. 1958. An experimental study of thermal convection in a rotating liquid. *Phil. Trans. Roy. Soc. London* (A) *250*, 441–478.

Kaiser, J. 1969. Rotating deep annulus convection. Part 1. Thermal properties of the upper symmetric regime. *Tellus 21*, 789–805.

Kuo, H. L. 1956. Energy releasing processes and stability of thermally driven motions in a rotating fluid. *J. Meteor. 13*, 82–101.

Lambert, R. B. & Snyder, H. A. 1966. Experiments on the effect of horizontal shear and change of aspect ratio on convective flow in a rotating annulus. *J. Geophys. Res. 71*, 5225–5234.

Lorenz, E. 1956. A proposed explanation for the existence of two regimes of flow in a rotating symmetrically heated cylindrical vessel. *Fluid Models in Geophysics. Proc. 1st Sympos. on the Use of Models in Geophysical Fluid Dynamics* (Baltimore, Md., Sept. 1953), pp. 73–80.

Lorenz, E. 1962. Simplified dynamic equations applied to the rotating basin experiments. *J. Atmos. Sci. 19*, 39–51.

Weil, J., Murty, T. & Rao, D. B. 1967. Zeros of $J_n(\lambda)\,Y_n(\eta\lambda) - J_n(\eta\lambda)\,Y_n(\lambda)$. *Math. of Comput. 21*, 722–727.

КОНВЕКЦИЯ В ГЛУБОКОМ ВРАЩАЮЩЕМСЯ КОЛЬЦЕВОМ СОСУДЕ.

Часть 2. Неустойчивость волн, вертикальная стратификация и соответствующие теории.

Дается обзор теорий бароклинной неустойчивости, имеющих отношение к дифференциально разогреваемым вращающимся кольцевым сосудам. Приводятся расчёты на их основе, выявляющие важность вертикальной стратификации жидкости. Представлены экспериментальные измерения нейтральной поверхности волнового режима, которые качественно согласуются с большинством предсказаний теории; в частности, получено хорошее согласие предсказанного эффекта вертикальной стратификации. Даются некоторые детали, касающиеся наблюдаемого перехода от волн с большой амплитудой к волнам с малой амплитудой. Представлено также некоторое экспериментальное указание на существование течений с одноволновой модой и смешанного течения с одно- и двухволновыми модами.